

# Percolation threshold gold films on columnar coatings: characterisation for SERS applications

Armandas Balčytis\*,<sup>1,2</sup> Tomas Tolenis\*,<sup>2</sup> Xuewen Wang,<sup>1</sup> Gediminas Seniutinas,<sup>1</sup> Ramutis Drazdys,<sup>2</sup> Paul R. Stoddart,<sup>3</sup> and Saulius Juodkazis<sup>1</sup>

<sup>1</sup>*Centre for Micro-Photonics, Swinburne University of Technology, John St., Hawthorn, VIC 3122, Australia*

<sup>2</sup>*State research institute Center for Physical Sciences and Technology, Savanorių ave. 231, Vilnius, Lithuania, LT-02300*

<sup>3</sup>*Faculty of Science, Engineering and Technology, Swinburne University of Technology, John St., Hawthorn, VIC 3122, Australia*

(Dated: October 1, 2018)

Percolation of gold films of  $\sim 15$  nm thickness was controlled to achieve the largest openings during Au deposition. Gold was evaporated on 300-nm-thick films of nanostructured porous and columnar SiO<sub>2</sub>, TiO<sub>2</sub> and MgF<sub>2</sub> which were deposited by controlling the angle, rotation speed during film formation and ambient pressure. The gold films were tested for SERS performance using thiophenol reporter molecules which form a stable self-assembled monolayer on gold. The phase retardation of these SERS substrates was up to 5% for wavelengths in the visible spectral range, as measured by Stokes polarimetry. The SERS intensity on gold percolation films can reach  $\sim 10^3$  counts/(mW·s) for tight focusing in air, while back-side excitation through the substrate has shown the presence of an additional SERS enhancement via the Fresnel near-field mechanism.

PACS numbers: Keywords: 3D coatings, Raman sensors, surface enhanced Raman scattering

## INTRODUCTION

It was demonstrated that optical near-field effects can be utilised to augment surface enhanced Raman scattering (SERS) intensity when light is traveling from the substrate (usually glass) into air or solution from where analyte molecules can attach to nano-islands of gold or other plasmonic metal [1]. This SERS excitation geometry is usually referred to as back-side whereas the standard retro-reflection setup with laser beam irradiating a substrate with metal nanoparticles from the air/solution side is the front-side.

Metal films nanometers in thickness deposited on different substrates have distinct formation morphologies defined by surface energy and deposition conditions. Percolation of individual islands takes place to form a film when thickness is typically exceeds 10 nm. Since back-side Raman excitation can increase SERS sensitivity by a factor of  $\propto n^4$  where  $n$  is the refractive index of the substrate (in reference to air or solution), it is of interest to explore properties of gold metal films at the percolation threshold, where interconnected metal islands produce the largest nano-groove openings. The possible polarisation effects on light transmission through a random pattern of nano-grooves, its coupling into surface plasmon polaritons, as well as plasmon localization effects are all very relevant for control of SERS performance. Recently, it was demonstrated that patterns of nanoparticles forming a metamaterial which can support

a traveling surface wave are better suited for SERS [3]. Also, randomness of a nanoparticle pattern in terms of their size and separation is advantageous for the spectrally broad-band performance and increased intensity in SERS [4, 5]. The percolation metal films studied here exhibit both randomness and surface interconnectivity.

When  $\sim \lambda/2$  waveplates are made out of dielectric layers deposited on a flat surface, it should be possible to achieve effective back-side irradiation field enhancement conditions using standard front-side illumination. For the  $\sim \lambda/2$  waveplate the phase shift of  $2\pi$  occurs for light which experiences reflection and a double pass in the film. By engineering reflectivity of the substrate and waveplate material with deposited gold films, SERS substrates can be realised with the added benefit of back-side augmentation of the local E-field of light. Such substrates can be straightforwardly used in upright Raman microscopy tools, whilst making use of an increased sensitivity. Complex 3D columnar coatings acting as waveplates have nano-rough surfaces when grown by glanced angle deposition. This feature has potential to be used for SERS after plasmonic metal coating.

Here, we report on the optical properties of gold films at the percolation threshold deposited on nanostructured SiO<sub>2</sub>, TiO<sub>2</sub> and MgF<sub>2</sub> coatings formed by glanced angle deposition and under low vacuum conditions for their use as SERS substrates. Such sensor surfaces are compatible with a practical fiber platform [6, 7].

## SAMPLES AND PROCEDURES

For experimental investigation six different samples were produced using a thin film deposition machine

---

\*\* authors who contributed equally.

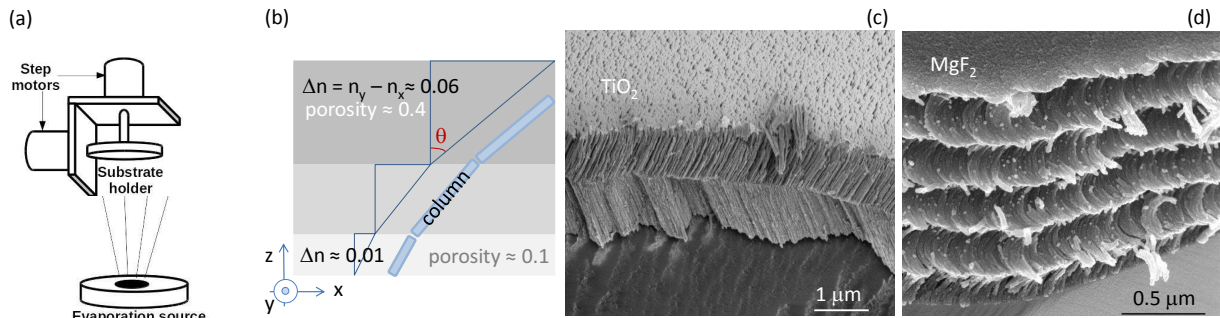


FIG. 1: Principle of glancing angle deposition. The orientation of the substrate is controlled by two step motors. An evaporation source is either an electron beam heated crucible with  $\text{Ti}_3\text{O}_5$  material or a resistively heated tungsten boat with  $\text{MgF}_2$  material. (b) Schematics of a columnar film grown by the glancing angle deposition with controlled porosity and birefringence  $\Delta n$  typical for  $\text{TiO}_2$  [2]. Cross sectional views of (c)  $\text{TiO}_2$  chevron films made at two different deposition angles and (d)  $\text{MgF}_2$  chiral waveplate made by glancing angle deposition with rotation.

VERA 1100 (VTD, Germany). All the films were prepared on a silica substrate by first coating dielectrics as the base layer and subsequently depositing gold on top of them. The inner structures and materials used for dielectric layers are summarized in Table I. Porosity in the dielectric films was due to intense gas-phase collisions in low  $P_0 = 10^{-1}$  Pa vacuum during transport from the source to the substrates [8]. The tilted columnar thin film (CTF) structure was formed by using the glancing angle deposition [9] technique which is used to make CTF and chiral films with controlled porosity and birefringence (Fig. 1(a,b)). The substrates were placed stationary above the evaporation source. By manipulating the substrate with dual step motors exceptional variety of achievable 3D film structures can be realized (Fig. 1(c,d)). As part of this work the angle between the vapour flux and the substrates was maintained at 60 or 70 degrees, depending on sample. For the **T60**\_ $\text{TiO}_2$  and **T70**\_ $\text{TiO}_2$  samples the evaporation source was  $\text{Ti}_3\text{O}_5$  material heated using an electron beam. A 300 nm thickness was coated at the evaporation rate of  $2\text{\AA}/\text{s}$ . In order to achieve complete oxidation, an additional oxygen flow of 20 sccm was introduced into the chamber. For the **V**\_ $\text{MgF}_2$  sample the evaporation source was  $\text{MgF}_2$  material placed in a resistively heated tungsten boat. For the production of vertical CTFs, the substrate was rotated about its axis at 1 rev/s. The remainder of the substrate geometry was kept the same. In CTF manufacturing cases the distance between the substrate and the evaporation source was maintained at 30 cm to ensure a collimated flux of vapour.

The top gold layer was evaporated in a separate process at the rate of  $0.5\text{\AA}/\text{s}$  for all the samples simultaneously. A thickness between 10 and 20 nm was formed using a resistive evaporator. A flat witness glass was used to control the process by monitoring the transmission at the wavelength of 600 nm. The evaporation process was stopped

TABLE I: Summary of the materials used for dielectric layers and their inner structure. The layers are porous (P), columnar tilted (T) and vertical (V). CTF = columnar thin film.

Sample	Structure	Material
<b>P</b> _ $\text{SiO}_2$	Porous	$\text{SiO}_2$
<b>P</b> _ $\text{MgF}_2$	Porous	$\text{MgF}_2$
<b>V</b> _ $\text{MgF}_2$	Vertical CTF	$\text{MgF}_2$
<b>T60</b> _ $\text{TiO}_2$	60° Tilted CTF	$\text{TiO}_2$
<b>T70</b> _ $\text{TiO}_2$	70° Tilted CTF	$\text{TiO}_2$
<b>V</b> _ $\text{TiO}_2$	Vertical CTF	$\text{TiO}_2$

when the transmission reached the first minimum due to the percolation effect (Fig. 2).

Polariscopy measurements were used to characterise the polarisation changes of light propagating through the columnar film and Au coating. The intensity of the transmitted light,  $I_T$ , was measured using a  $\lambda/4$  waveplate and an analyser at different orientational angles  $\beta$  and  $\alpha$ , respectively, according to [10]:

$$I_T(\alpha, \beta) = 1/2[I + (Q \cos(2\beta) + U \sin(2\beta)) \cos(2(\alpha - \beta)) + V \sin(2(\alpha - \beta))], \quad (1)$$

where  $\alpha$  and  $\beta$  are the rotation angles of the fast axis of the polarizer and the waveplate with respect to the  $x$ -axis (horizontal).

The four Stokes parameters,  $S(I, Q, U, V)$ , that define an arbitrary state of light polarisation, are determined by separate measurements with the waveplate and analyser

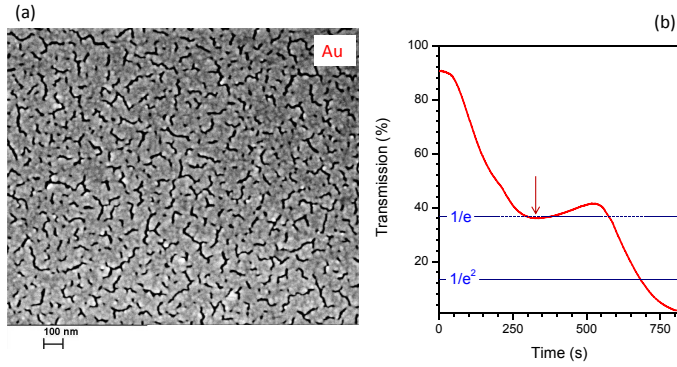


FIG. 2: (a) Gold film at the percolation threshold evaporated on the  $\text{SiO}_2$  porous film (sample  $\text{P-SiO}_2$ ). (b) Transient of transmission monitored during gold deposition. Arrow mark represents the condition of film shown in (a).

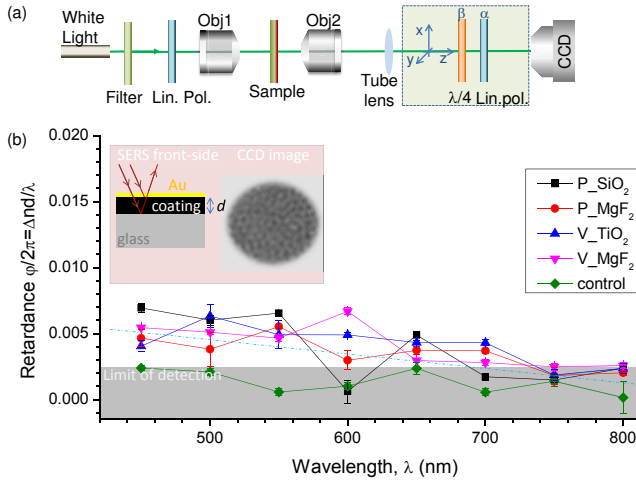


FIG. 3: (a) Schematic of the setup used to measure Stokes parameters  $S(I, Q, U, V)$  and retardance  $\varphi = \text{atan}(V/U)$ . (b) Retardance,  $\varphi$ , spectra presented in wavelength fractions  $\varphi/2\pi = \Delta nd/\lambda$  for different samples with porous and columnar films (Table I); 1-mm-thick silica was used as a control sample. Inset shows schematics of the front-side SERS measurements and a CCD image of a  $\sim 50 \mu\text{m}$ -diameter area on the sample which was integrated in order to determine the Stokes parameters. Error bars are  $\pm 30\%$ . The dashed line is prediction of a linear dependence  $\varphi \propto d/\lambda$ .

at fixed angles of  $\alpha$  and  $\beta$ , given by:

$$\begin{aligned}
 I &= I_T(0, \pi/4) + I_T(0, -\pi/4), \\
 Q &= 2I_T(0, 0) - I, \\
 U &= 2I_T(\pi/4, \pi/4) - I, \\
 V &= 2I_T(0, -\pi/4) - I.
 \end{aligned}
 \tag{2}$$

It is usual to present Stokes parameters as the Poincaré sphere with the retardation given by  $\varphi = \text{atan}(V/U)$ .

Filters of 10 nm spectral bandwidth were used to select different central wavelengths from a white-light super-continuum laser (SuperK Compact, NKT Photonics) in

the range from 400 to 800 nm and focused to a  $5 - 7 \mu\text{m}$  spot on the sample. The incident linearly polarised light was set at 45 degree polarization using a Glan-Taylor polarizer and was focused onto a region of the sample via an objective lens of numerical aperture  $NA = 0.26$  ( $10\times$ , Mitutoyo). After the sample, an  $NA = 0.5$  objective lens ( $100\times$ , Mitutoyo) was used to collect and collimate the transmitted light for polarisation analysis. The sample and the two objectives were mounted on 2D positioning stages. Polarisation analysis was carried out after the second objective with an achromatic  $\lambda/4$ -waveplate and a second Glan-Taylor polarizer. Phase retardation,  $\varphi$ , of the  $45^\circ$  linear polarized beam (i.e. the phase delay between the  $s$ - and  $p$ -polarized light) was measured as  $\varphi = 2\pi\Delta nd/\lambda$ , where  $\Delta n$  is the birefringence,  $d$  is the thickness of the structure (a film with Au coating), and  $\lambda$  is the wavelength of light. A tube lens and a  $1024 \times 768$  pixel CCD were used for imaging and transmission measurements. Typical lateral resolution was  $5 - 7 \mu\text{m}$ . The setup was tested by measuring retardance of a commercial  $\lambda/2$ -plate.

Raman scattering spectra were acquired using an InVia Streamline Raman microscope (Renishaw, UK) under  $\lambda = 633 \text{ nm}$  continuous wave laser excitation at  $P = 2.94 \text{ mW}$  total power, focused with an objective lens of numerical aperture  $NA = 0.25$ . The Au layer was functionalized by immersing the substrates for 30 min in a 10 mM ethanolic thiophenol solution. Substrates were subsequently rinsed in ethanol, to remove thiophenol molecules not bound to Au, and blow-dried with  $\text{N}_2$ . Near-field enhancement effects were probed by performing Raman spectra acquisitions, both, with laser incidence from the thin-film deposition side (front-side) and by focusing on the Au layer through the 4 mm-thick glass substrate (back-side).

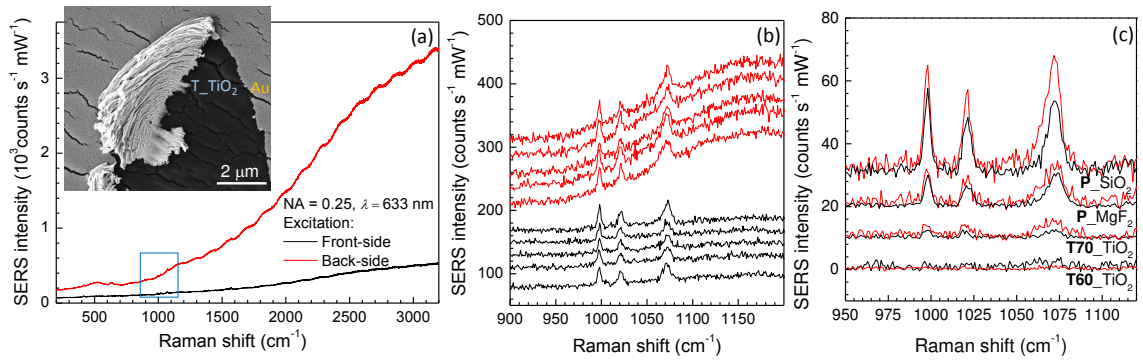


FIG. 4: Raman scattering spectra of thiophenol measured on  $\sim 15$  nm thick Au via front-side and back-side acquisition at several locations. (a) Broad-sweep Raman spectra obtained on sample **P\_SiO<sub>2</sub>** and exhibiting increased background scattering for the  $\sim 4$  mm thickness glass substrate. Weak thiophenol signature is shown in the region-of-interest box; Inset shows a typical SEM image of surface used for SERS: Au on the CTF film. (b) Close-up view of thiophenol spectral lines measured on sample **P\_SiO<sub>2</sub>** in top-side and back-side acquisition cases. (c) Comparison of background subtracted Raman signal obtained on different dielectric coatings underlying the thin Au film at the percolation threshold. Objective lens was  $NA = 0.25$ , wavelength of excitation  $\lambda = 633$  nm, acquisition time 5 s. See Table I for sample nomenclature.

## RESULTS AND DISCUSSION

For SERS functionality nano-particles and nano-gaps are essential for light field enhancement at nanoscale - the generation of “hot-spots”. Gold films at the percolation threshold have a random pattern of openings, hence, nano-gaps which can be used as hot-spots in SERS. Figure 2(a) shows a typical Au film coated over a SiO<sub>2</sub> porous layer (sample **P\_SiO<sub>2</sub>**). This surface morphology corresponds to the local minimum in the transmission observed during deposition (Fig. 2(b)) and is also observed when TiO<sub>2</sub> and MgF<sub>2</sub> underlying dielectric coatings are used. Thickness of the gold film was 10-20 nm as could be estimated from SEM images. Gold was evaporated directly onto the porous or CTFs and was loosely attached to the substrate. A local transmission minimum occurs when transmission,  $T$ , is approximately at a  $1/e$ -level (for the normalised transmission). The refractive index of gold at  $\lambda = 600$  nm is  $n + ik = 2.42 + i2.9152$ , hence, the transmission through a thickness of  $x = 16.5$  nm is  $T = \exp(-4\pi kx/\lambda) \simeq 1/e$ . For longer gold deposition durations there is at first a slight increase in transmission, most probably due to an augmented forward scattering through the openings as result of Fresnel reflection, before  $T$  starts to continuously decrease once the openings are closed and the gold film grows in thickness.

Columnar coatings deposited at large glancing angles exhibit nanoscale surface roughness and by applying a thin Au coating they were prepared for SERS. Polariscopy measurements were carried out to characterise the retardance of the coating with Au film at the percolation threshold. Figure 3 shows that an effective retardance measured in transmission was only 0.2-0.5% of the corresponding wavelength over the entire visible spectrum. This is a very small number and the porous and colum-

nar films served only as nano-rough substrates for SERS. It is noteworthy, that coatings corresponding to  $\lambda/2$  retardance would realise phase matching for constructive interference on the Au surface (inset in Fig. 3) and can be used to augment SERS intensity (planned as a next step of this study). The light reflected from the glass-coating boundary (inset in Fig. 3) can be considered as a back-side SERS excitation component, since it is propagating from the high to the low refractive index region, hence, the Fresnel enhancement takes place [1]. Thickness of the coating,  $d$ , was measured from SEM cross sectional images and was  $d \simeq 300 \pm 10$  nm, which defines the birefringence  $\Delta n \simeq 6 \times 10^{-3}$  for the measured  $\varphi/2\pi = 0.003$  at  $\lambda = 633$  nm used in SERS. Intriguingly, a very small birefringence was observed in the case of porous and vertical columnar structures (Fig. 3) for which isotropic, hence non-birefringent, film performance is expected. However, film deposition is a complex process governed by local temperature and material delivery peculiarities, hence, local symmetry breaking and anisotropy can be expected and related to the material flux. For example, surface of the vertical columnar film (Fig. 1(d)) clearly shows an anisotropy of nano-grain orientation on the top of the film. Thicker dielectric films will be made for experimental measurements of birefringence and will be related to the cross sectional morphology and porosity in a following study.

Low SERS signals were observed from thiophenol reporter molecule coated samples (Fig. 4). The back-side irradiation mode showed a strong fluorescence background (Fig. 4(a)). The region-of-interest for thiophenol peaks on porous silica **P\_SiO<sub>2</sub>** for the front- and back-side SERS collection modes is shown in (Fig. 4(b)). There was a recognisable difference between SERS intensity for the two acquisition modes. The SERS intensity is nor-

malised only to the transmission through the microscope and a front-side reflection is not taken into account for the data shown in Fig. 4 for the back-side mode (reflectivity of the air-surface is  $R = (n - 1)^2 / (n + 1)^2$  for intensity). A slightly larger SERS signal by a factor of 1.2-1.6 was observed for the back-side irradiation. The reason of the enhancement is due to the local E-field amplitudes being different in the surface for the air-substrate and substrate-air cases [1]. For example, in the case of glass substrate for a back-side mode the amplitude of the transmitted light depends on the refractive index ratio between media of incidence and transmission ( $n_i = 1.5$  vs  $n_t = 1$ ) as  $t = 2n_i / (n_i + n_t) \equiv 1.2$ . Since SERS enhancement factor depends on the local E-field intensity at the wavelength of excitation and scattering - the electromagnetic enhancement factor,  $M_{Enh}$  - one can expect an augmented SERS intensity by a factor of  $M_{Enh} = I_{exc}^2 \times I_{Raman}^2 \simeq t^4 \simeq 2.1$ . The strongest back-side enhancement was observed for a silica porous film which has a slightly larger refractive index than porous MgF<sub>2</sub>: for a solid film it would correspond to 1.4 vs 1.2. Interestingly, tilted column TiO<sub>2</sub> films (deposition at 60 and 70 degrees) showed almost identical SERS intensity for both modes of excitation, most likely due to the negligible difference in retardance in both cases over the 300 nm thickness. However, for the CTF structures, there is a possibility to control the local light field intensity on the interface where SERS is measured by the phase control through film thickness and exploiting the zero phase shift for light traversing from the higher to lower refractive index region ( $n_t < n_i$ ).

Earlier studies showed that SERS intensity is proportional to the thickness of gold [11, 12] for measurements in reflection (front-side mode). Formation of hot-spots in SERS occurs when 3D morphology of the surface develops in thicker gold films. If gold is coated over existing 3D nano-textured surfaces the hot-spots are formed in the crevices as demonstrated for well controlled 3D surface patterns [13]. In this regard the percolation nanogaps are not as directly applicable for SERS since they are mostly planar and formed on a flat substrate. SERS is typically measured on 100-nm-thick Au coatings and up to 6-8 fold decrease in SERS intensity is expected on 16 nm gold films. SERS intensity is also scales linearly with the solid collection angle and a low numerical aperture  $NA = 0.25$  (cone angle  $\psi = 14.5^\circ$ ) used in back-side SERS measurements contributes to the lower signal [14]. The observed SERS rate of 30 counts/(mW·s) would be 3 times stronger for the popular  $NA = 0.75$  (cone angle  $\psi = 48.5^\circ$ ) acquisition mode. This shows that the layer system of nanostructured dielectric and thin gold films used in this study can perform at the level of  $10^3$  counts/(mW·s) for the commonly used  $NA = 0.75$  lens which is typical for many reported SERS substrates. Further SERS enhancement is achievable with formation of deep nano-grooves usually obtained on nano-rough

substrates using thick ( $d > 100$  nm) metal coatings.

## CONCLUSIONS AND OUTLOOK

It has been demonstrated that thin  $\sim 15$  nm gold coatings at the percolation threshold can be used as SERS substrates. Re-scaled for acquisition with a typical  $NA = 0.75$  objective lens, the SERS intensity could reach  $10^3$  counts/(mW·s), which is typical in the SERS field. The presence of the back-side SERS intensity augmentation is confirmed for percolation films for the first time.

Future work is required for fabricating SERS substrates which are optimised for maximum E-field enhancement factors on the surface via the use of birefringent CTF  $\lambda/2$  plates and percolation coatings. Phase control via the thickness of the phase plate could bring a new means of SERS control [15] and can be implemented to improve the signal-to-noise ratio using SERS signals from two different CTF regions. Such control would inherently require a percolation property of films for light transmission. Porosity and gas permeability of CTF could also find use in practical SERS applications.

## Acknowledgements

SJ is grateful for partial support via the Australian Research Council Discovery project DP130101205 and a sensor technology transfer project with Workshop of Photonics Ltd.

- 
- [1] S. Jayawardhana, L. Rosa, S. Juodkakis, and P. R. Stodart, "Additional enhancement of electric field in surface-enhanced Raman scattering due to Fresnel mechanism," *Sci. Rep.* **3**, p. 2335, 2013.
  - [2] G. J. Lee, Y. P. Lee, B. Y. Jung, S. G. Jung, C. K. Hwangbo, J. H. Kim, and C. K. Yoon, "Microstructural and nonlinear optical properties of thin silver films near the optical percolation threshold," *J. Korean Phys. Soc.* **51**(4), pp. 1555 – 1559, 2007.
  - [3] A. V. Kabashin, P. Evans, S. Pastkovsky, W. Hendren, G. A. Wurtz, R. Atkinson, R. Pollard, V. A. Podolskiy, and A. V. Zayats, "Plasmonic nanorod metamaterials for biosensing," *Nature Materials* **8**, pp. 867 – 871, 2009.
  - [4] Y. Nishijima, Y. Hashimoto, L. Rosa, J. B. Khurgin, and S. Juodkakis, "Scaling rules of SERS intensity," *Adv. Opt. Mat.* **2**(4), pp. 382–388, 2014.
  - [5] Y. Nishijima, J. B. Khurgin, L. Rosa, H. Fujiwara, and S. Juodkakis, "Randomization of gold nano-brick arrays: a tool for SERS enhancement," *Opt. Express* **21**(11), pp. 13502–13514, 2013.
  - [6] A. K. Sharma, R. Jha, and B. D. Gupta, "Fiber-optic sensors based on surface plasmon resonance: a compre-

- hensive review,” *Sensors Journal IEEE* **7**(8), pp. 1118–1129, 2007.
- [7] P. R. Stoddart and D. J. White, “Optical fibre SERS sensors,” *Anal. Bioanal. Chem.* **394**(7), pp. 1761 – 1774, 2009.
- [8] A. Lakhtakia and R. Messier, *Sculptured thin films: Nanoengineered Morphology and Optics*, SPIE Press, Bellingham, Washington USA, 2005.
- [9] R. Messier, T. Gehrke, C. Frankel, V. C. Venugopal, W. Otano, and A. Lakhtakia, “Engineered sculptured nematic thin films,” *J. Vac. Sci. Technol. A* **15**(4), pp. 2148–2152, 1997.
- [10] H. G. Berry, G. Gabrielse, and A. E. Livingston, “Measurement of the Stokes parameters of light,” *Applied Optics* **16**(12), pp. 3200 – 3205, 1977.
- [11] R. Buividas, P. R. Stoddart, and S. Juodkazis, “Laser fabricated ripple substrates for surface-enhanced Raman scattering,” *Annalen der Physik* **524**(11), pp. L5 – L10, 2012.
- [12] A. Balčytis, M. Ryu, G. Seniutinas, J. Juodkazytė, B. C. C. Cowie, P. R. Stoddart, J. Morikawa, and S. Juodkazis, “Black-CuO: Surface-enhanced Raman scattering and infrared properties,” *Nanoscale* **7**(43), pp. 18299–18304, 2015.
- [13] S. Dinda, V. Suresha, P. Thoniyot, A. Balčytis, S. Juodkazis, and S. Krishnamoorthy, “Engineering 3D nanoplasmonic assemblies for high performance in spectroscopic sensing,” *ACS Appl. Mater. Interf.* **7**(50), pp. 27661 – 27666, 2015.
- [14] S. Jayawardhana, L. Rosa, R. Buividas, P. R. Stoddart, and S. Juodkazis, “Light enhancement in surface-enhanced Raman scattering at oblique incidence,” *Photonic Sensors* **2**(3), pp. 283–288, 2012.
- [15] A. N. Grigorenko, P. I. Nikitin, and A. V. Kabashin, “Phase jumps and interferometric surface plasmon resonance imaging,” *Appl. Phys. Lett.* **75**(25), pp. 3917–3919, 1999.